First-Order Liquid-Liquid Phase Transition in Cerium

A. Cadien,[1,*] Q. Y. Hu,[1] Y. Meng,[2] Y. Q. Cheng,[3] M. W. Chen,[4] J. F. Shu,[5] H. K. Mao,[2,5] and H. W. Sheng[1,6,†]

[1]School of Physics, Astronomy and Computational Sciences, George Mason University, Fairfax, Virginia 22030, USA
[2]High Pressure Collaborative Access Team, Geophysical Laboratory, Carnegie Institution of Washington, Argonne, Illinois 60439, USA
[3]Chemical and Engineering Materials Division, Oak Ridge National Laboratory, Oak Ridge, Tennessee 37831, USA
[4]WPI Advanced Institute for Materials Research, Tohoku University, Sendai 980-8577, Japan
[5]Geophysical Laboratory, Carnegie Institution of Washington, Washington, DC 20015, USA
[6]Center for Computational Materials Science, George Mason University, Fairfax, Virginia 22030, USA

(Received 20 November 2012; published 21 March 2013)

We report the first experimental observation of a liquid-liquid phase transition in the monatomic liquid metal cerium, by means of *in situ* high-pressure high-temperature x-ray diffraction experiments. At 13 GPa, upon increasing temperature from 1550 to 1900 K high-density liquid transforms to a low-density liquid, with a density difference of 14%. Theoretic models based on *ab initio* calculations are built to investigate the observed phase behavior of the liquids at various pressures. The results suggest that the transition primarily originates from the delocalization of f electrons and is deemed to be of the first order that terminates at a critical point.

DOI: 10.1103/PhysRevLett.110.125503 PACS numbers: 61.20.−p, 31.15.bu, 61.05.C−, 71.22.+i

The liquid counterpart to crystalline polymorphism is of great importance to the understanding of the liquid state and the formation of matter but has not been well studied [1–4]. Theoretical models as well as computer simulations have predicted the existence of liquid-liquid phase transitions (LLPT) in several systems [5–10]. Liquid polyamorphism has been suggested to exist in liquids involving directional bonding [11], typical examples being water [4,6,7], silicon [9,10], fused quartz [12] and molecular liquids [13–16]; nonetheless, there exist few unambiguous laboratory demonstrations of LLPT thus far [17].

Experimental observation of LLPT, manifested by large density changes of different liquid forms with the same chemical makeup, necessitates studies across a wide temperature-pressure phase space (e.g., high temperatures and high pressures). In addition to the thermodynamic obstacles, experimental observation of LLPT involves several complications [18]. For example, the LLPT in water may lie in an experimentally inaccessible region of the phase diagram, preventing a direct observation of the transition in the stable liquid [19]. There is also difficulty involved in the structural demarcation of different liquid forms because of the lack of lattice periodicity in liquid states. As such, successful experimental investigations of LLPT are exceedingly rare. Herein, relying on high-temperature high-pressure x-ray diffraction techniques, we report our discovery of liquid polyamorphism in a monatomic metallic system—cerium (Ce).

Ce exhibits the first recorded isomorphic transition from cF4 (fcc, γ) to the cF4 (fcc, α) phase with a large volume collapse of up to 17% [20–24]. This phase boundary terminates at a critical point, where the volume collapse diminishes. The cause for this unusual transition is the dual valency states of Ce of which f electrons participate in bonding under applied pressures [20,22]. In conjunction with the peculiar V-shaped melting curve in the T-P phase diagram [23] the possibility of a hidden LLPT in Ce is suggested.

In this work, the melting process and liquid behavior of Ce at various pressures are studied by x-ray diffraction (XRD) at the High-Pressure Collaborative Access Team (HPCAT), 16-IDB, at the Advanced Photon Source. *In situ* high-intensity XRD was employed to monitor the structural evolution of Ce under high pressures and high temperatures. The diamond-anvil-cell technique was used to generate pressure in the range of $0 \sim 30$ GPa, and a double-sided *in situ* laser heating system allows access to a temperature range up to several thousand Kelvin under high pressures. X-ray scattering data were collected and recorded on a MAR345 image plate detector. At low pressures (1.9 GPa), the experiments were performed using argon as the pressure media and thermal insulation and the ruby florescence method was used for pressure calibration. At high pressures (13, 22 GPa) MgO was used as insulating layers between sample and diamond anvils, and the equation of state of MgO was used for pressure calibration. The melting process was identified by the appearance of diffusive halolike diffraction patterns and the disappearance of sample diffraction lines. After integration of the 2D imaging plate, the raw 1D signals (as a function of momentum transfer) were processed and converted into structure factors using inhouse software. The structure factors of Ce melt were extracted from the diffraction patterns by separating the remaining crystalline peaks of the pressure media and a small amount of Ce oxides.

The *ab initio* calculations [25] are based on the generalized gradient approximation with the Perdew-Burke-Ernzerhof [26] parametrization for the exchange-correlation functional to density-functional theory. We adopted the projected augmented wave approach [27] as implemented in the Vienna *ab initio* simulation package (VASP) [25]. A first-principles database was established by performing extensive *ab initio* calculations that span over a large phase space of Ce, and the database augmented with experimental data was used to extract many-body embedded-atom-method (EAM) [28] interatomic potentials for Ce by employing the force-matching method [29]. The accuracy and performance of the EAM potentials can be found in the Supplemental Material [30]. The free energies of the liquids were obtained with the thermodynamic integration method (see Supplemental Material [30]).

At room temperature, the detected polymorphic transitions of Ce [30] are found to be consistent with the phase diagram, with a general trend showing the phase evolution of $(\gamma \rightarrow \alpha \rightarrow \alpha'' \rightarrow \epsilon)$ [24] with increasing pressures. XRD patterns of the melting sequence at each pressure are recorded, confirming the pressure range in which our experiments were conducted.

The XRD patterns of Ce melt at 1.9, 13, and 22 GPa are shown in Fig. 1. At these three pressures, the behavior of XRD evolution with increasing temperature shows different characteristics. At 1.9 GPa, no obvious shift of the main diffraction peak was found (except for a small peak shift resulting from thermal expansion), suggesting that the structure of the liquid phase is rather stable at this pressure. At 13 GPa a shoulder emerges and grows from the low-q side of the main diffraction peak at the cost of the old peak with increasing temperature until a new diffraction peak takes form, whose position [$q = 2.46$ Å^{-1} at 1900 K; see Fig. 1(c)] differs significantly from that of the melt at low temperatures ($q = 2.34$ Å^{-1} at 1500 K). This drastic peak shift suggests a large atomic density difference in the melt. An estimate based on the ratio of the peak positions for the two liquid phases indicates a volume collapse of ~14%. These results show that a high-density liquid (HDL) to low-density liquid (LDL) transition occurred in Ce. At 22 GPa the main diffraction peak undergoes a gradual and continuous shift from $q = 2.52$ Å^{-1} at 1430 K to $q = 2.46$ Å^{-1} at 1600 K. Upon quenching to room temperature, the melt transforms back to the crystalline phases at corresponding experimental pressures. More details of the peak position shift as a function of temperature at the three pressures can be found in the Supplemental Material [30].

Reference structures corresponding to the different pure valence states of Ce are introduced which allow a computational study of the experimentally observed HDL and LDL phases. These were obtained through classical molecular dynamics employing newly developed high-fidelity EAM potentials designed to model trivalent Ce^{f_0} and tetravalent Ce^{f_1} metals. By juxtaposing the structure factors of Ce^{f_0} and Ce^{f_1} liquids with the experimental results, as shown in Fig. 1, one can observe that at low pressures (1.9 GPa), the structure of the melt is close to that of the Ce^{f_0} liquid; at 13 GPa, the structures of the experimentally observed HDL and LDL are close to those of the Ce^{f_1} and Ce^{f_0} liquid, respectively. At 22 GPa, the experimental structure factors of Ce liquids appear to be similar to that of the high-density Ce^{f_1} liquid, and they gradually shift toward that of the low-density Ce^{f_0} liquid with an increase in the temperature.

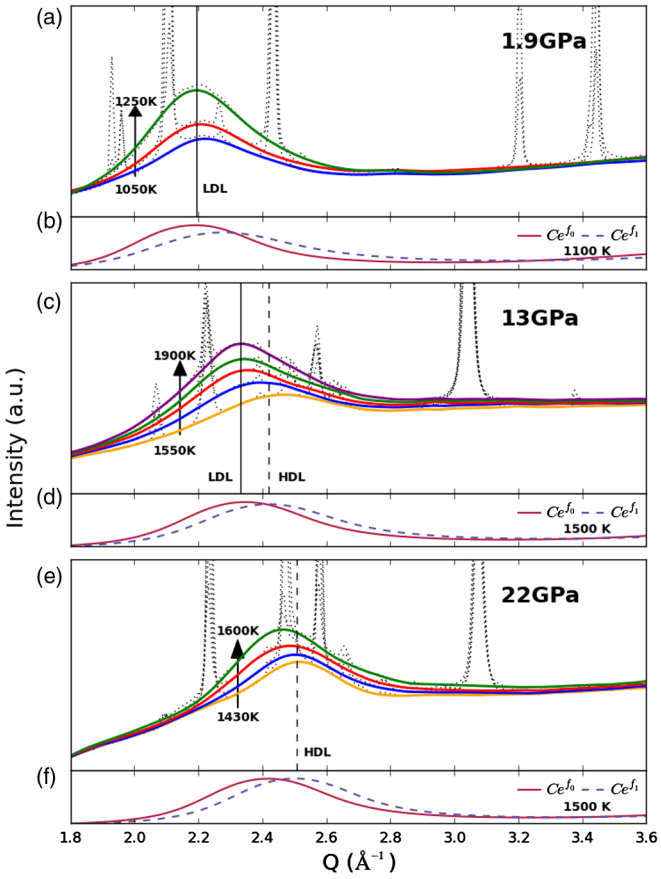

FIG. 1 (color online). X-ray diffraction patterns for cerium at a range of pressures and temperatures (a), (c), (e). Dotted lines are raw experimental data from which the liquids (solid lines) are extracted; the crystal peaks present are discussed in the Supplemental Material [30]. The diffraction intensities are scaled to better illustrate the phase evolution of liquid Ce. In (b), (d), and (f) the structure factors from EAM simulations of the two reference Ce liquids are shown.

The atomic structures of Ce^{f_0} and Ce^{f_1} liquids are further differentiated in Fig. 2, by the *ab initio* radial distribution functions of the liquid inherent structures [31]. Features uncommon to most liquid metals are present in the Ce^{f_1} radial distribution function; it displays a split first peak. Because of the core-softening phenomenon caused by the delocalization and screening of f electrons, two characteristic bonding lengths (2.9, 3.5 Å) are observed at low pressures. The long bonds in Ce^{f_1} are pressure dependent and shrink as pressure increases in contrast to the short

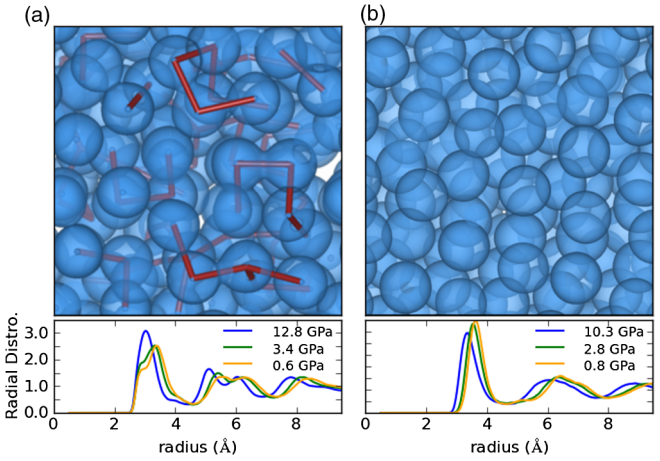

FIG. 2 (color online). Charge density isosurfaces from *ab initio* simulations (top) and radial distribution functions (bottom) for Ce^{f_1} (a) and Ce^{f_0} (b) at a range of pressures. The simulations were performed on the liquid inherent structures of Ce liquids quenched from 1500 K. The short bonds present in Ce^{f_1} liquids are shown as solid rods, corresponding to the shoulder centered at 2.9 Å at 0.6 GPa in the radial distribution function. The results have been reproduced with large-scale molecular dynamics simulations by employing the EAM potentials.

bonds which are resilient. Similar phenomena have been reported for simulated liquids by exploiting two-scale potential models [7,8,32]. For the low-density Ce^{f_0} liquid, the liquid structure is typical of most simple liquid metals, and it can be approximated as a hard-sphere ensemble.

Liquid Ce may assume a mixed valence state in the experiment, depending on the degree of f-electron localization, which may bear a resemblance to the electronic configuration of Ce across the $\gamma \leftrightarrow \alpha$ volume collapse transition. It should be noted that the exact electronic origin of the $\gamma \leftrightarrow \alpha$ structural transition has been under intense research for many years [33–35], and two prevailing models attempt to understand the behavior of f-electron interactions, i.e., the Mott-transition model [33] and the Kondo volume collapse model [34]. In this work, interpretation of the phase behavior of liquid Ce under high pressure was attempted based on the Mott-transition model.

In the spirit of the Mott-transition treatment [22] of Ce, the mixed valence state of Ce can be modeled with $Ce^{f_0}_{1-x}Ce^{f_1}_{x}$ pseudoalloys. By using this treatment, we can analyze the thermodynamic conditions for the LLPT of Ce by assessing the free energy of the pseudoalloy. By adopting Aptekar-Ponyatovsky's regular solution model [36], the Gibbs free energy of liquid Ce is expressed as

$$g(P,T,x) = (1-x)g_0(P,T) + xg_1(P,T) + u_{\mathrm{mix}}x(1-x) + k_BT[x\ln(x) + (1-x)\ln(1-x)],$$

where $g_0(P,T)$ and $g_1(P,T)$ are the per-atom Gibbs free energies of pure Ce^{f_0} and Ce^{f_1} liquids, respectively, x is composition, u_{mix} is the heat of mixing, and k_B is the Boltzmann constant. The free energies g_0 and g_1 are computed using the thermodynamic integration method by employing the EAM potentials. It is important to note that, when calculating the free energy of the Ce^{f_0} phase, g_0, one has to consider the additional contribution of electronic and magnetic entropies, S_{em}, due to the extra spin degree of freedom afforded by the localized f electrons on the Ce^{f_0} atoms [22,37]. Following Ref. [37], an empirical form of

$$S_{\mathrm{em}} = \ln(8)k_B + 0.0004k_BT$$

accounts for the magnetic and electronic entropy of Ce^{f_0}. The heat of mixing, u_{mix}, is found to be weakly dependent on pressure and temperature, and a constant value of 370 meV/atom is employed. The computed Gibbs free energies of liquid Ce at the experimental P and T are plotted in Fig. 3 as a function of composition. The phase selection of LDL and HDL is easily discernible from the locations of the free-energy minima, corroborating the experimental observation of the stable LDL phase at 1.9 GPa and the HDL phase at 22 GPa. At 13 GPa, a first-order LLPT is expected to occur at the temperature where the two free-energy minima are equal, which is indeed what is observed in Fig. 1. The phase equilibrium temperatures of the two liquid phases at each pressure can be derived as shown in Fig. 3(d). The two energy minima on the free-energy curves correspond to the LDL and the HDL phases with different concentrations of Ce^{f_0} and Ce^{f_1} states in the liquid phases. Below 6 GPa the equilibrium LDL and HDL phases are predominantly pure Ce^{f_0} and Ce^{f_1} states, respectively. The HDL and LDL branches of

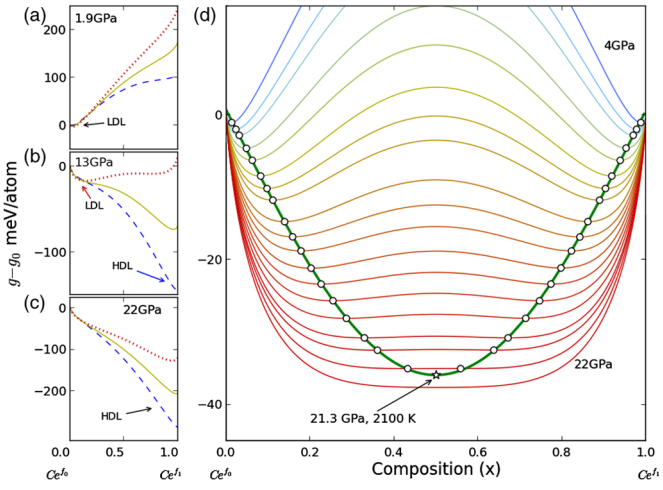

FIG. 3 (color online). (a), (b), (c) Free-energy curves at the pressures corresponding to experiments and temperatures at 1200, 1500, and 1800 K and 1800 K which are dashed, solid, and dotted lines, respectively. (d) Free energy along the LLPT curve increases from 4 (blue) to 22 GPa (red) by 1 GPa increments. White circles and the fitted green line highlight the compositions ($Ce^{f_0}_{1-x}Ce^{f_1}_{x}$) of the LDL and HDL liquids, which lead to a liquid-liquid critical point at 21.3 GPa and 2100 K.

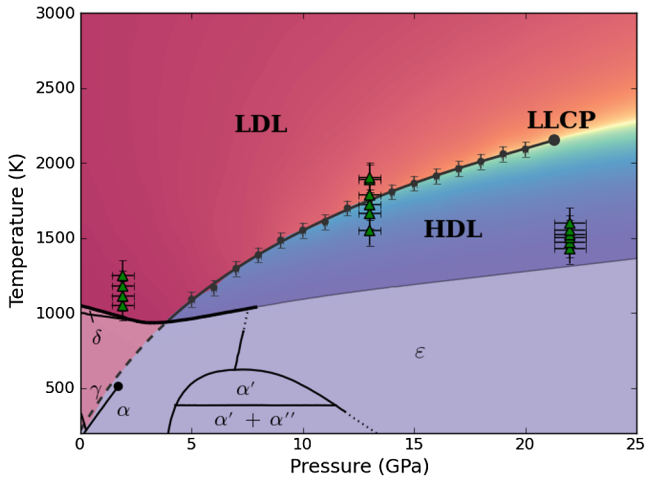

FIG. 4 (color online). Ce Phase diagram [23] overlaid on the LDL-HDL phase boundary estimated from free-energy calculations. The LLPT is highlighted by a thick gray line and ends at a liquid-liquid critical point near 21.3 GPa and 2100 K as derived in Fig. 4. The transition curve is dashed in the supercooled region. The temperature and pressure of experimentally observed liquids are shown as green triangles. Only diffraction patterns that exhibit a strong liquid halo were used.

the free energy converge as the pressure increases, leading to the occurrence of a critical point. Above the critical pressure, the free-energy curves always exhibit one minimum, indicating that the first-order transition between LDL and HDL no longer exists.

The central experimental and computational results can be demonstrated from the P-T phase diagram of Ce, with new information about the LLPT of Ce shown in Fig. 4. The phase boundary of the LLPT has a positive slope dT/dP. In the equilibrium liquid, it rises from the V-shaped dip of the melting curve at 3.2 GPa and terminates at a critical point. While the LLPT observed in Fig. 1 is entropy and thereby temperature dependent, it may also be density driven by modulating the pressure under an isothermal condition. The latter is confirmed by our experiment at ~1100 K that LDL Ce at 1.9 GPa transforms to HDL Ce at 4.0 GPa (see Supplemental Material [30]). The extrapolated phase boundary in the supercooled region is close to the $\gamma \leftrightarrow \alpha$ isostructural phase transition boundary [21].

Pure liquid metals can hardly be supercooled far below their melting point such that direct observation of Ce polyamorphism in the supercooled state may be difficult. Nonetheless, alloying Ce with other metals may enhance the forming ability of glasses. Metallic glasses containing Ce may serve as a surrogate for the investigation of liquid polyamorphism [38]. Such polyamorphic transitions have been observed in Ce-based metallic glasses [39,40], which are consistent with the extrapolated LLPT in Fig. 4. Moreover, the recent discovery of polymorphic transitions in a series of lanthanide-based bulk metallic glasses [41] suggests the LLPT is common to systems prone to large electronic configuration changes (e.g., 4f electron delocalization). Therefore, our report on the LLPT of Ce will not only shed light on the liquid state of metals but also open avenues to study the physics of the formation of new materials.

The work was supported by U.S. NSF under Grant No. DMR-0907325 and ONR under Grant No. N00014-091-1025A. H. K. M. was supported as part of EFree, an Energy Frontier Research Center funded by the U.S. Department of Energy, Office of Science, Office of Basic Energy Sciences under Award No. DE-SC0001057. Y. Q. C. was supported at ORNL by Scientific User Facilities Division, DOE-BES. The authors thank E. Ma and T. Frolov for their assistance at the early stage of the project, and thank T. Fujita for his help with the computational work. HPCAT operations are supported by CIW, CDAC, UNLV, and LLNL through funding from DOE-NNSA and DOE-BES, with partial instrumentation funding by NSF. The computational work was conducted on the SR10000-K1/52 supercomputing facilities of the Institute for Materials Research, Tohoku University.

*Corresponding author.
acadien@gmu.edu
†Corresponding author.
hsheng@gmu.edu

[1] D. Chandler, Proc. Natl. Acad. Sci. U.S.A. **106**, 15111 (2009).
[2] P. H. Poole, T. Grande, C. A. Angell, and P. F. McMillan, Science **275**, 322 (1997).
[3] C. A. Angell, Science **267**, 1924 (1995).
[4] L. Liu, S. H. Chen, A. Faraone, C. W. Yen, and C. Y. Mou, Phys. Rev. Lett. **95**, 117802 (2005).
[5] S. Sastry and C. A. Angell, Nat. Mater. **2**, 739 (2003).
[6] P. H. Poole, F. Sciortino, U. Essmann, and H. E. Stanley, Nature (London) **360**, 324 (1992).
[7] G. Franzese, G. Malescio, A. Skibinsky, S. V. Buldyrev, and H. E. Stanley, Nature (London) **409**, 692 (2001).
[8] L. Xu, P. Kumar, S. V. Buldyrev, S.-H. Chen, P. H. Poole, F. Sciortino, and H. E. Stanley, Proc. Natl. Acad. Sci. U.S.A., **102**, 16558 (2005).
[9] V. V. Vasisht, S. Saw, and S. Sastry, Nat. Phys. **7**, 549 (2011).
[10] P. Ganesh and M. Widom, Phys. Rev. Lett. **102**, 075701 (2009).
[11] R. Kurita and H. Tanaka, Science **306**, 845 (2004).
[12] I. Saika-Voivod, F. Sciortino, and P. H. Poole, Phys. Rev. E **63**, 011202 (2000).
[13] Y. Katayama, Y. Inamura, T. Mizutani, M. Yamakata, W. Utsumi, and O. Shimomura, Science **306**, 848 (2004).
[14] V. V. Brazhkin, Y. Katayama, M. V. Kondrin, T. Hattori, A. G. Lyapin, and H. Saitoh, Phys. Rev. Lett. **100**, 145701 (2008).
[15] V. V. Brazhkin, I. Farnan, K. Funakoshi, M. Kanzaki, Y. Katayama, A. G. Lyapin, and H. Saitoh, Phys. Rev. Lett. **105**, 115701 (2010).

[16] G. D. Mukherjee and R. Boehler, Phys. Rev. Lett. **99**, 225701 (2007).
[17] Y. Katayama, T. Mizutani, W. Utsumi, O. Shimomura, M. Yamakata, and K. Funakoshi, Nature (London) **403**, 170 (2000).
[18] P. F. McMillan, M. Wilson, M. C. Wilding, D. Daisenberger, M. Mezouar, and G. N. Greaves, J. Phys. Condens. Matter **19**, 415101 (2007).
[19] O. Mishima and H. E. Stanley, Nature (London) **396**, 329 (1998).
[20] D. G. Koskenmaki and K. A Gschneidner, Jr., *Handbook on the Physics and Chemistry of Rare Earths* (Elsevier, New York, 1979), Vol. I, p. 337.
[21] M. J. Lipp, D. Jackson, H. Cynn, C. Aracne, W. J. Evans, and A. K. McMahan, Phys. Rev. Lett. **101**, 165703 (2008).
[22] B. Johansson, I. A. Abrikosov, M. Alden, A. V. Ruban, and H. L. Skriver, Phys. Rev. Lett. **74**, 2335 (1995).
[23] A. Schiwek, F. Porsch, and W. B. Holzapfel, High Press. Res. **22**, 407 (2002).
[24] M. I. McMahon and R. J. Nelmes, Phys. Rev. Lett. **78**, 3884 (1997).
[25] G. Kresse and J. Hafner, Phys. Rev. B **49**, 14251 (1994).
[26] J. P. Perdew, K. Burke, and M. Ernzerhof, Phys. Rev. Lett. **77**, 3865 (1996).
[27] P. E. Blochl, Phys. Rev. B **50**, 17953 (1994).
[28] M. S. Daw and M. I. Baskes, Phys. Rev. B **29**, 6443 (1984).
[29] H. W. Sheng, M. J. Kramer, A. Cadien, T. Fujita, and M. W. Chen, Phys. Rev. B **83**, 134118 (2011).
[30] See Supplemental Material at http://link.aps.org/supplemental/10.1103/PhysRevLett.110.125503 for details of experimental methods and analysis, explanations of semiempirical potential, and free-energy calculations.
[31] F. H. Stillinger and T. A. Weber, Phys. Rev. A **25**, 978 (1982).
[32] P. C. Hemmer and G. Stell, Phys. Rev. Lett. **24**, 1284 (1970).
[33] B. Johansson, Philos. Mag. **30**, 469 (1974).
[34] J. W. Allen and R. M. Martin, Phys. Rev. Lett. **49**, 1106 (1982).
[35] M. J. Lipp, A. P. Sorini, J. Bradley, B. Maddox, K. T. Moore, H. Cynn, T. P. Devereaux, Y. Xiao, P. Chow, and W. J. Evans, Phys. Rev. Lett. **109**, 195705 (2012).
[36] I. L. Aptekar and E. G. Ponyatovsky, Fiz. Met. Metalloved. **25**, 777 (1968).
[37] M. Lüders, A. Ernst, M. Däne, Z. Szotek, A. Svane, D. Ködderitzsch, W. Hergert, B. L. Györffy, and W. M. Temmerman, Phys. Rev. B **71**, 205109 (2005).
[38] C. A. Angell, *Structural Glasses and Supercooled Liquids: Theory, Experiment, and Applications* (Wiley, New York, 2011), p. 250.
[39] H. W. Sheng, H. Z. Liu, Y. Q. Cheng, J. Wen, P. L. Lee, W. K. Luo, S. D. Shastri, and E. Ma, Nat. Mater. **6**, 192 (2007).
[40] Q. S. Zeng *et al.*, Proc. Natl. Acad. Sci. U.S.A. **104**, 13565 (2007).
[41] G. Li, Y. Y. Wang, P. K. Liaw, Y. C. Li, and R. P. Liu, Phys. Rev. Lett. **109**, 125501 (2012).